International Journal of Mass Spectrometry 281 (2009) 8–14

Contents lists available at ScienceDirect

International Journal of Mass Spectrometry

journal homepage: www.elsevier.com/locate/ijms

An IT-TOF mass spectrometer for the analysis of organic aerosol

Julie A. Lloyd, Murray V. Johnston*

Department of Chemistry and Biochemistry, University of Delaware, Newark, DE 19716, USA

ARTICLE INFO

Article history:
Received 10 September 2008
Received in revised form 4 November 2008
Accepted 5 November 2008
Available online 14 November 2008

Keywords:
Ion trap time-of-flight mass spectrometer
Organic aerosol
Laser desorption ionization
Laser desorption–electron ionization
Matrix-assisted laser desorption ionization

ABSTRACT

An ion trap time-of-flight (IT-TOF) mass spectrometer has been developed for online analysis of organic aerosol. Airborne particles are focused through an aerodynamic lens assembly and deposited onto a stainless steel collection probe inserted through a hole in the ring electrode of an ion trap. The collected sample is desorbed and ionized with a pulsed 355-nm Nd:YAG laser beam within the ion trap cavity. Ions are collisionally cooled to the center of the trap prior to extraction into a reflectron time-of-flight mass analyzer. Relative to a previous version of the instrument without an ion trap, incorporation of the ion trap increases the sensitivity and resolution of ions that are formed directly at the probe surface and permits post-ionization with electrons to be performed. Online analysis of perylene and C_{60} test aerosols were performed by one-step laser desorption ionization (LDI). Online analysis of secondary organic aerosol (SOA) from α-pinene ozonolysis was performed by laser desorption–electron ionization (LD–EI). Matrix-assisted laser desorption ionization (MALDI) was also performed, and the molecular ion signal was enhanced with a dynamic RF trapping method.

1. Introduction

Aerosol mass spectrometry has become a powerful tool for characterizing the time-resolved chemical composition of ambient aerosol [1–3]. Atmospheric particles span a wide range of size (1 nm to 100 μm) and composition (both organic and inorganic components). Particle sources, whether biogenic or anthropogenic, can often be inferred from a specific size/composition signature. The initial composition subsequently may change as the particle undergoes transformation and reaction in the atmosphere. As a result, both particle size and composition vary substantially with time. Understanding this variation is important as ambient aerosol can significantly impact global climate [4,5] and human health [6].

Many aerosol mass spectrometers couple laser desorption ionization (LDI) with time-of-flight mass analyzers, although other methods such as thermal desorption (TD) followed by electron ionization (EI) or chemical ionization (CI), and two-step laser desorption/ionization are also employed [2,3]. Ionization methods are selected based on the type of species that will be analyzed and therefore determine the type of chemical information that is obtained. For example, LDI is used for single particle analysis when a wide variety of components, both inorganic and organic, semivolatile and refractory, must be detected. When studying specific organic species in ambient aerosol, alternative soft ionization techniques are needed to reduce the amount of fragmentation of the molecular ion.

The photoionization aerosol mass spectrometer (PIAMS) previously developed in our laboratory employs a two-step laser desorption/ionization method for soft ionization of organic compounds [7,8]. An aerosol sample is collected on a probe, typically for a couple of minutes. After collection, the sample is laser desorbed with a pulsed infrared laser beam. After a set time delay, the plume of desorbed, neutral molecules is softly ionized by coherent vacuum ultraviolet radiation (VUV PI) at 118 nm (10.5 eV) and analyzed with a reflectron time-of-flight (TOF) mass spectrometer. The PIAMS configuration facilitates analysis of low concentration components since aerosol is collected over a period of time and analyzed all at once. The configuration is also well suited for 2-step LDI owing to the pulsed nature of a TOF analyzer. The spatial and temporal distributions that cause peak broadening in TOF MS are minimized by the short (<5 ns) VUV pulse width and the small cross-section of the plume that is irradiated. VUV PI is generally regarded as a soft, universal ionization method and has proven useful for identifying and tracking sources of ambient organic aerosol based on the signal intensities of specific marker compounds [8]. Although molecular ion intensities are generally large with VUV PI, substantial fragmentation can occur which can make a detailed spectral interpretation difficult [9]. For this reason, a desired capability is the use of other ionization modes, especially those that can reduce fragmentation further and/or selectively detect targeted species.

Replacing the conventional source region of the current PIAMS instrument with a quadrupole ion trap (IT) provides greater flexibility for ionization. Ion traps have been interfaced with a variety

* Corresponding author. Tel.: +1 302 831 8014 fax: +1 302 831 6335.
E-mail address: mvj@udel.edu (M.V. Johnston).

1387-3806/$ – see front matter © 2008 Elsevier B.V. All rights reserved.
doi:10.1016/j.ijms.2008.11.001

of in-source ionization techniques such as EI, CI, and one-step LDI including matrix-assisted laser desorption ionization (MALDI) [10]. Incorporation of MALDI into the PIAMS configuration would provide the opportunity to characterize molecular components in biological particles [11–13]. Incorporation of EI into the PIAMS configuration would permit rapid switching between soft and hard ionization modes. Soft ionization allows specific molecular marker compounds to be monitored while hard ionization provides a global characterization of complex aerosol samples, for example distinguishing hydrocarbon-like and oxygenated organic aerosol (HOA and OOA, respectively) in ambient air [14].

The ion trap time-of-flight (IT-TOF) configuration was first developed by Lubman and co-workers using 266 nm radiation to perform laser-induced resonance enhanced multiphoton ionization (REMPI) of gas phase organic compounds [15]. The laser beam entered and exited the trap through holes in the ring electrode. Ions formed inside the trap were stored and then extracted into a TOF analyzer. Chambers et al. used a similar IT-TOF design for analysis of gaseous compounds, but created ions by chemical ionization [16]. In their study, N_2 and O_2 from air served as the ionization agent as well as the buffer gas for cooling the ions to the center of the trap. This instrumental design allowed for the real-time monitoring of trace volatile and semivolatile compounds in air. For the analysis of non-volatile compounds, LDI [17] and MALDI [18] have been performed with an IT-TOF configuration by manually spotting the sample on a probe and inserting it into a hole in the ring electrode. Several other groups have used a similar probe design for LDI in a conventional IT mass spectrometer [19–26]. In this work, the IT-TOF configuration is explored for aerosol analysis using several ionization modes.

2. Experimental methods

Fig. 1 shows the IT-TOF analyzer for aerosol collection and analysis. The configuration is similar to PIAMS [7] except that the conventional TOF source assembly is replaced by an IT. The aerosol passes through an aerodynamic lens assembly that forms a particle beam. The particle beam enters the IT through a hole in the ring electrode and strikes a collinearly aligned stainless steel collection probe (diameter ~2.3 mm) that fits through a second hole in the opposite side of the electrode. When inserted, the probe fits flush with the electrode surface and does not distort the RF field [19]. The probe also contacts the ring electrode, therefore it is held at the same potential as the ring electrode. The probe design is similar to PIAMS in that a flat, roughened surface is used to minimize particle bounce and enhance the signal detected [7]. After sample has been accumulated on the probe, a pulsed laser fires and irradiates the probe surface by passing through the apertures of the aerodynamic lens assembly. In this work, 355 nm radiation from a Nd:YAG laser (New Wave Research, Inc., Fremont, CA) is used for one-step desorption ionization of collected samples. Since the laser beam is unfocused, only about 30% of the output radiation strikes the probe. Pulse energies between 0.25 and 1.2 mJ across an area of ~2.5 mm^2 at the probe surface were used depending on the experiment.

Laser desorbed ions were subjected to a 10-ms cooling period inside the IT using helium at a local pressure between 10^{-4} and 10^{-3} Torr. The IT (r_o = 10 mm, z_o = 7.1 mm; Jordan TOF Products, Inc., Grass Valley, CA) was operated at an RF drive frequency of 1.17 MHz with an adjustable amplitude of 0–2500 $V_{p\text{-}p}$. During the cooling period, the end caps were held at ground potential. Ion extraction into the TOF was performed by turning off the RF drive frequency and applying symmetric potentials to the end caps (+950 V/−950 V). The end cap potentials were applied for a 5.0-μs pulse width that began 3–5 μs after the RF potential was removed. The ions were accelerated into a reflectron time-of-flight mass analyzer (Jordan TOF Products, Inc., Grass Valley, CA) and the signal from a microchannel plate detector was digitized at a rate of 500 MHz by two 8-bit channels (DP235 Acqiris, Geneva, Switzerland) with overlapping scales with different sensitivities to maximize the dynamic

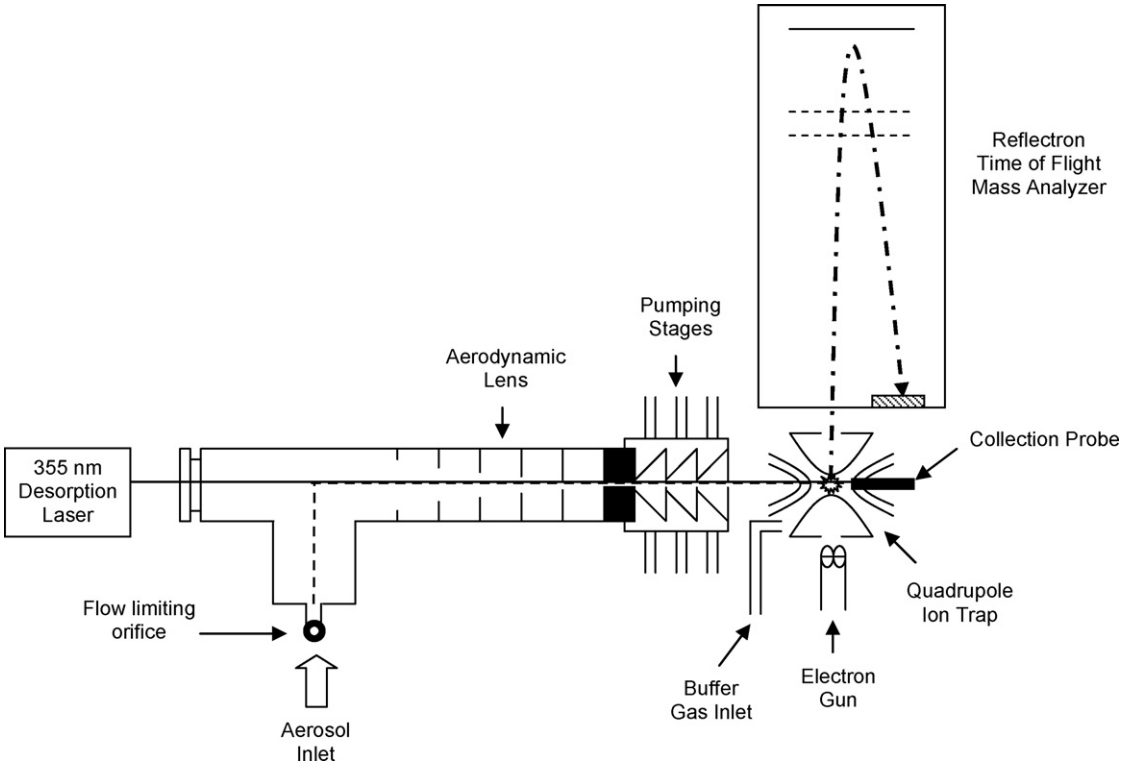

Fig. 1. Schematic of the IT-TOF mass spectrometer.

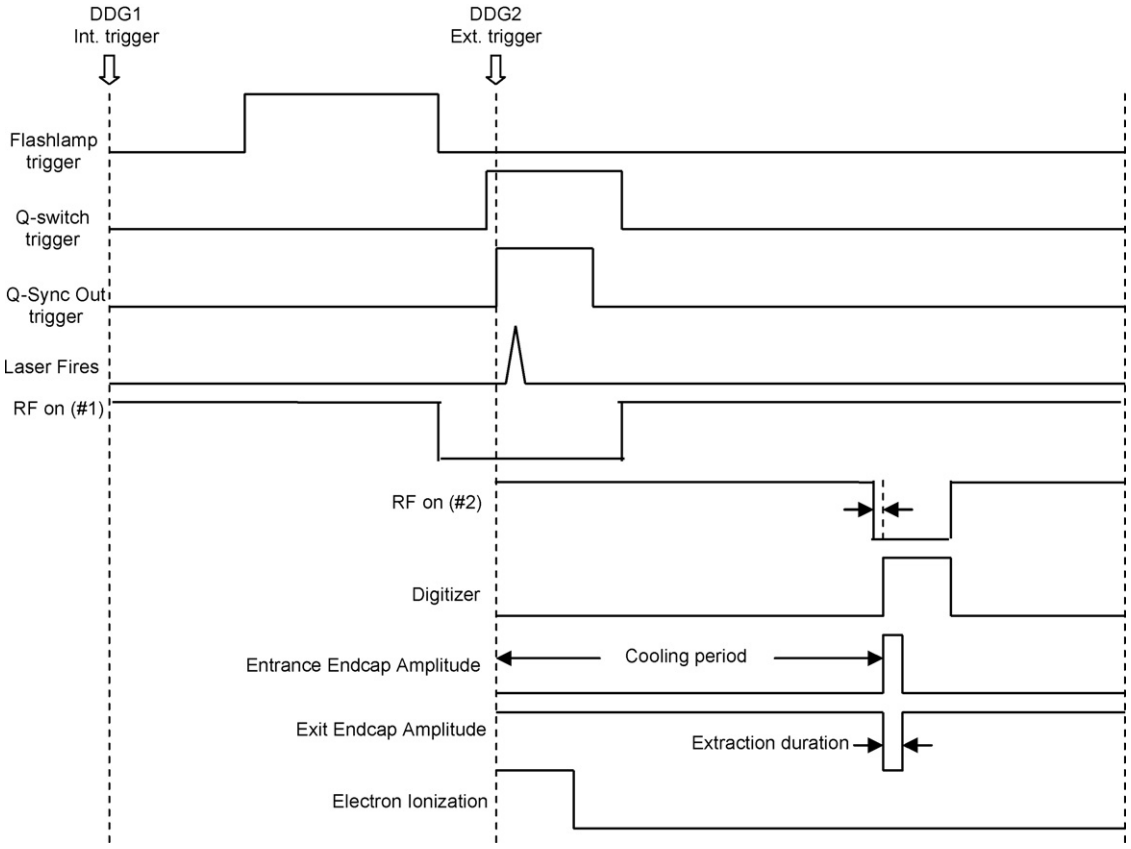

Fig. 2. Timing diagram showing the sequence for laser firing and the various modes of IT-TOF operation. Diagram is not drawn to scale.

range. The ionization, cooling and analysis steps were repeated at a 10-Hz rate to remove all sample from the probe. LabView 8.2 software (National Instruments, Austin, TX) controlled instrument operation and data processing.

Fig. 2 shows the timing diagram for laser firing and IT-TOF operation. Two digital delay generators (DDG) (DG535, Stanford Research Systems, Sunnyvale, CA) controlled the timing sequence of events. The first DDG triggered the Nd:YAG laser and the shut-off for the RF potential (#1), which was typically set to internally trigger at a rate of 10 Hz. The laser flashlamp and Q-switch triggers were offset by 190 μs to maximize the laser pulse energy. The second DDG was externally triggered by the laser Q-Sync output and controlled the shut-off for the RF potential (#2), the collisional cooling period, the time when potentials were applied to the end caps to extract ions into the TOF analyzer, and signal acquisition by the digitizer.

With this setup, three different experiments could be performed: (1) orthogonal extraction TOF MS, (2) IT-TOF MS with continuous RF trapping, and (3) IT-TOF MS with dynamic RF trapping. In addition, an electron gun (70 eV) was pulsed to perform EI of laser desorbed neutrals in the continuous RF trapping mode. In the orthogonal extraction experiment, the RF potential was disabled (i.e., the ring electrode was held at ground) and the end cap potentials were pulsed at a specific time delay after the laser pulse. In the continuous trapping experiment, the RF potential remained on as the laser was fired, and was disabled only when ions were extracted into the TOF (indicated by #2 in Fig. 2). In the dynamic trapping experiment, the RF potential was turned off twice, first just prior to the laser pulse (indicated by #1 in Fig. 2) and second when ions were extracted into the TOF. For each RF turn-off, the RF potential decayed to 0 $V_{p\text{-}p}$ within 5 μs and remained at the baseline for a time period of about 20 μs. After this time period, the RF amplitude increased approximately linearly with time over ~120 μs to reach its specified value. The laser was not synchronized to the RF phase in either continuous or dynamic RF trapping experiments.

Polydisperse aerosols were generated with a constant output atomizer (Model 3076, TSI, Inc., St. Paul, MN). The aerosols were neutralized and dried in a diffusion dryer (Model 3062, TSI Inc., St. Paul, MN). Number and mass concentrations were determined using a scanning mobility particle sizer (SMPS) (DMA model: 3081, CPC model: 3025, TSI Inc., St. Paul, MN). Solutions of perylene and buckministerfullerene (C_{60}) were prepared in hexanes at concentrations of 0.02 and 0.012 mg/mL, respectively. Secondary organic aerosol (SOA) from α-pinene ozonolysis was generated in a flow tube reactor that has been described previously [27]. Some experiments were also conducted by manually spotting samples onto the probe. A 10 mg/mL solution of α-cyano-4-hydroxycinnamic acid (CHCA) was prepared in acetonitrile/0.1% TFA water (70:30, v/v). Leucine enkephalin was prepared in deionized water (Millipore, Bedford, MA) at a concentration of 0.292 mg/mL to give a matrix-to-analyte ratio of 100:1. Matrix and peptide were spotted in a 1:1 (v/v) ratio and were allowed to dry prior to insertion into the vacuum system. Leucine enkephlin was obtained from Anaspec, Inc. (San Jose, CA), solvents were obtained from Fisher (Fair Lawn, NJ), and all other chemicals were obtained from Sigma–Aldrich (St. Louis, MO).

3. Results and discussion

3.1. Orthogonal extraction TOF MS

The ion kinetic energy distribution has a significant impact on trapping efficiency in an IT. The ion velocity can be estimated from

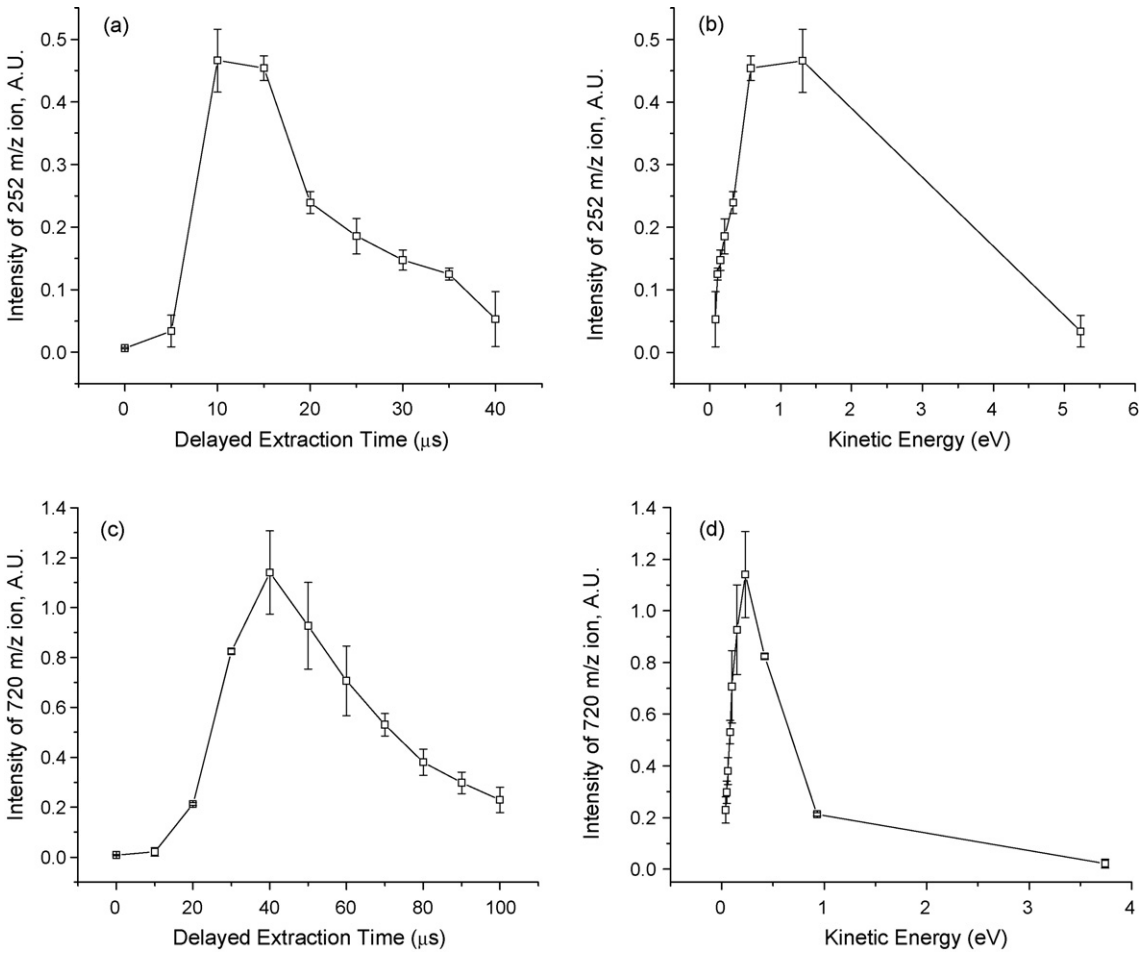

Fig. 3. Signal intensities of the 252 m/z and 720 m/z ions as a function of the delayed extraction time (a) and (c) as well as a function of kinetic energy (b) and (d).

an orthogonal extraction TOF experiment where the ring electrode is held at ground, no buffer gas is leaked into the trap, and the end cap potentials are pulsed to initiate ion extraction into the TOF with a characteristic time delay relative to the laser pulse. During this time delay, ions move from the probe surface toward the center of the trap. Since the size of the aperture in the end cap is small, ions can escape into the TOF only if they have traveled to a location near the center of the trap. Fig. 3(a) and (c) shows the ion signal intensity as a function of the time delay between ion formation (laser pulse) and ion extraction (end cap potential pulse) for perylene (252 m/z) and C_{60} (720 m/z), respectively. The signal intensity for perylene reaches a maximum between 10 and 15 μs, which corresponds to an ion velocity between 667 and 1000 m/s if the ions must travel approximately 10 mm to reach the center of the trap in order to be sensitively detected. The signal intensity for C_{60} reaches a maximum at 40 μs, corresponding to a velocity of 250 m/s. Fig. 3(b) and (d) shows the kinetic energy distributions for these ions based on the delay time dependencies and distance traveled. Most perylene ions have kinetic energies below 2 eV and most C_{60} ions below 1 eV. As discussed below, these energies are well below the pseudopotential well depth, which suggests that efficient ion trapping is possible.

3.2. Continuous trapping with LDI and EI

Fig. 4 shows the LDI mass spectra of aerosol deposited perylene by orthogonal extraction and continuous ion trapping. Fig. 4(a) shows the orthogonal extraction TOF mass spectrum taken under the same conditions as Fig. 3 with a 10-μs delay between ion formation and extraction. The resulting signal was relatively weak and poorly resolved since the radial kinetic energy distribution is large. When the RF potential was engaged with a 2400-$V_{p\text{-}p}$ amplitude and the trap was filled with 10^{-3} to 10^{-4} Torr helium, the ion signal intensity increased by a factor of 4 and the baseline resolution improved by a factor of 2 (Fig. 4(b)). This improvement is due to the collisional cooling, which reduces the spatial and energy distributions inherent to LDI. A similar improvement is observed in the C_{60} spectrum. The trapping efficiencies and hence signal intensities of both samples were strongly dependent on RF amplitude. The lowest amplitude to give a detectable signal was about 300 $V_{p\text{-}p}$, which corresponds to a pseudopotential well depth (D_r) in the radial direction of 0.4 eV for perylene and 0.14 eV for C_{60}. These values are not surprising given the ion kinetic energy distributions in Fig. 3. Larger signals and greater well depths were achieved with a RF amplitude of 2400 $V_{p\text{-}p}$, which corresponds to well depths of 25.5 and 8.9 eV, respectively, for perylene and C_{60}.

On the order of 100 pg sampled through the inlet was found to give a detectable signal (SNR ≥ 3). Under normal operating conditions for ambient measurements (2 min. sample deposition, 0.1 L/min aerosol sampling rate, 30× aerosol concentrator prior to sampling), this would correspond to an aerosol mass concentration of ~20 ng/m^3 [8]. It should be noted that not all of the sampled material was deposited on the probe due to particle bounce off the probe surface and particle beam broadening associated with the nonspherical particle morphologies of the aerosols studied. Furthermore, the current system yields a laser beam smaller than the probe area, so not all of the deposited aerosol is irradiated. Therefore, there are several avenues for future improvements in detection.

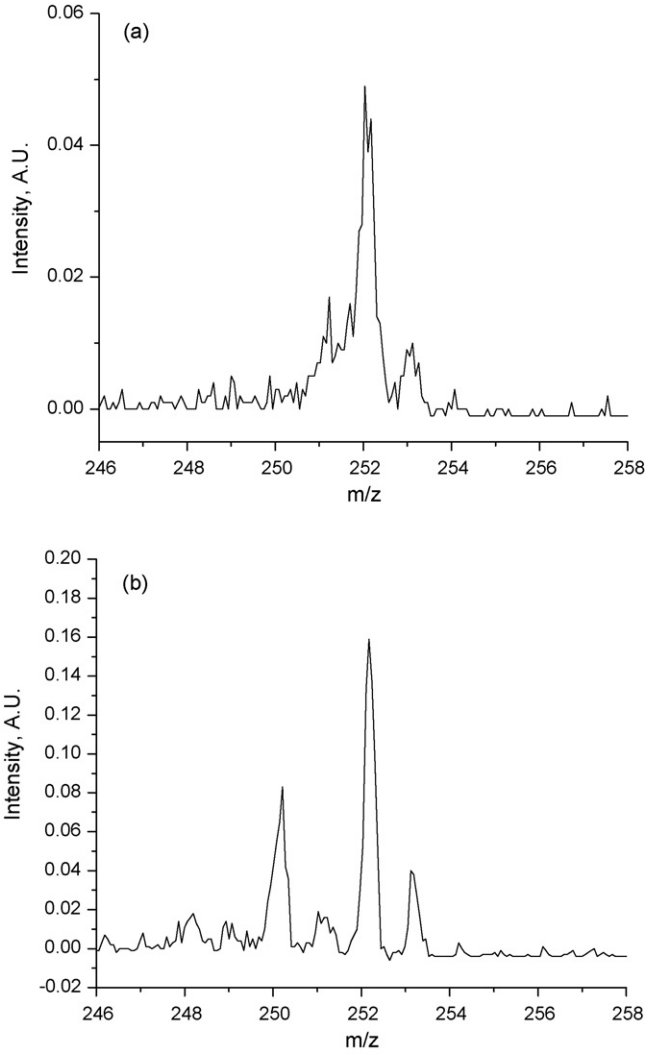

Fig. 4. LDI averaged mass spectra of aerosol deposited perylene by (a) orthogonal extraction TOF MS and (b) continuous ion trapping at an RF amplitude of 2400 $V_{p\text{-}p}$.

An interesting feature of Fig. 4(b) is the additional ion at 250 *m*/*z*, which corresponds to the loss of H_2 from the molecular ion. This fragmentation is apparently induced during operation of the ion trap since it is missing from Fig. 4(a). The interplay between ion trapping and dissociation are studied further in the next section.

In addition to the LDI experiments described above, EI was initially demonstrated using C_{60} aerosol. With a relatively low ionization potential of 7.6 eV, C_{60} aerosol could be desorbed and ionized at 355 nm yielding an intense molecular ion ($C_{60}^{+\bullet}$). When the electron gun was turned on, a second intense ion at 360 *m*/*z* appeared in the mass spectrum (data not shown). This ion correlates to the doubly charged molecular ion (C_{60}^{2+}), which is a major ion in the 70 eV NIST library spectrum.

Additional LD–EI experiments were performed with the online deposition of α-pinene SOA. In this case, no ionization occurred as a result of the 355 nm irradiation step. Fig. 5 shows the EI mass spectrum of α-pinene SOA sampled through the aerodynamic inlet at RF amplitude 1000 $V_{p\text{-}p}$. This RF amplitude sets the low mass cut-off to be approximately 35 *m*/*z* in order to eliminate interferences of N_2 and O_2 as background gases in the ion trap. The dominant ions in the spectrum are found at 39, 41, and 43 *m*/*z* correlating to aliphatic species that may or may not be oxygenated. Aliphatic ion series are also observed at 55, 69, 83, 97, 111, 125 *m*/*z* as well as 53, 67, 81, 95, 109 *m*/*z*. The EI mass spectrum correlates well with smog chamber

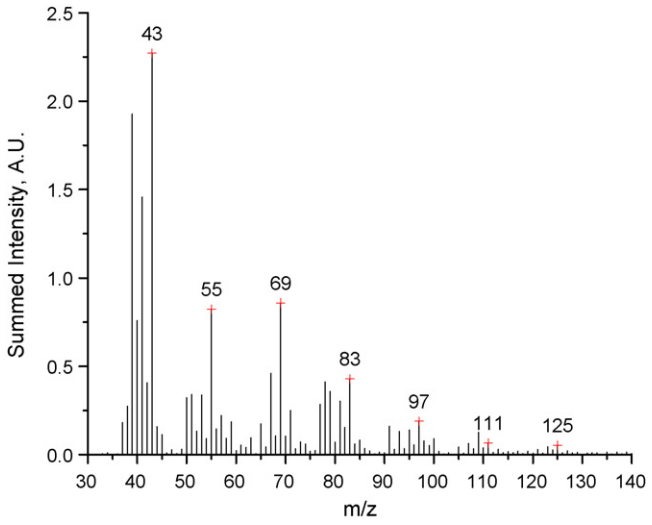

Fig. 5. LD–EI mass spectrum of α-pinene SOA sampled for a 20-min period using continuous RF trapping at an RF amplitude of 1000 $V_{p\text{-}p}$.

α-pinene SOA data reported using thermal vaporization (600 °C)–EI [28]. The one major difference between thermal vaporization–EI and LD–EI is the substantially higher intensity of the 44 *m*/*z* ion in thermal vaporization experiments relative to LD–EI in Fig. 5. This difference suggests that the 44 *m*/*z* ion, a key indicator of the oxygen content of SOA [29], is produced by thermal decomposition of the aerosol followed by EI of gas phase CO_2 and that the amount of CO_2 produced is strongly dependent on the vaporization conditions. In the present work, it appears that laser desorption from a relatively cool probe is not as likely to result in pyrolysis to form CO_2 as thermal desorption from a hot probe. Changing the probe material to porous tungsten or the laser wavelength to 1064 nm had no effect on the intensity of the 44 *m*/*z* ion.

3.3. Dynamic trapping with MALDI

MALDI has been successfully interfaced with an ion trap using either radial ion introduction [16,19,23,24] or more commonly, axial ion introduction [30–32]. In the work described here, the matrix and analyte are manually spotted on the probe surface. Morphological effects associated with aerosol deposition will be reported separately. Fig. 6(a) shows a MALDI mass spectrum of leucine enkephalin (MW 555 g/mol) using CHCA matrix (MW 189 g/mol) with continuous RF trapping at 2400 $V_{p\text{-}p}$. Peptides are commonly observed in the MALDI spectra of biological particles [11–13]. Most of the peaks in the mass spectrum are less than 200 *m*/*z* and correlate to matrix peaks as well as peptide fragment ions. Specifically, the immonium ions for phenylalanine (F) at 120 *m*/*z* and tyrosine (Y) at 136 *m*/*z* were detected with relatively high signal intensities. The most intense peaks at 115 *m*/*z* and 116 *m*/*z* correlated to the low molecular mass fragment ions of GG and z_1, respectively. Other less intense peaks at 91, 132 and 221 *m*/*z* correlated to the protonated phenylalanine side chain, y_1, and b_2 fragment ions, respectively. One intense peak greater than 200 *m*/*z* was detected at 318 *m*/*z*; however, the identity of the ion is unclear. This ion may correlate to a sodium cation of the c_3 fragment ion, a potassium cation of the y_2 fragment ion, or a loss of H_2O from the y_3 fragment ion. No molecular ion of leucine enkephalin was detected as others have previously reported using a similar laser desorption setup within the ion trap [21,25,26]. When sampling only matrix, analyte peaks were not detected as expected. Intense matrix peaks in the mass spectrum correlate to the matrix molecular ion $[CHCA–H]^+$ and

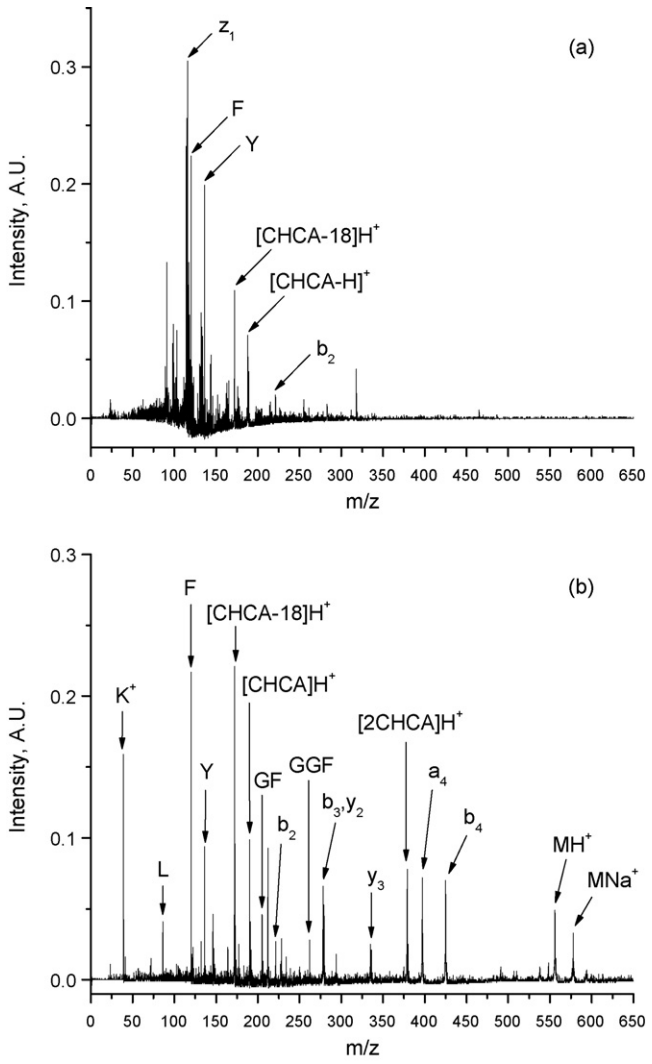

Fig. 6. Mass spectrum of leucine enkephalin with CHCA matrix using (a) constant RF potential at RF amplitude of 2400 $V_{p\text{-}p}$ and (b) dynamic RF trapping at RF amplitude of 600 $V_{p\text{-}p}$. Each spectrum represents 50 laser shots averaged.

the loss of water from CHCA [CHCA-18 Da]H^+ at 188 and 172 m/z, respectively.

Dynamic RF trapping [22,23] was employed to further investigate MALDI spectra in the IT-TOF configuration. Fig. 6(b) shows a MALDI mass spectrum of leucine enkephalin with CHCA matrix where the RF field was turned off and remained at the baseline when the laser fired. The RF amplitude then increased linearly to the set value of 600 $V_{p\text{-}p}$ as the ions traveled to the center of the trap. Like the continuous RF mass spectrum in Fig. 6(a), the most intense peaks were less than 200 m/z; however, in this case higher m/z ions were also detected. Several intense fragment ions and internal ions of leucine enkephalin were found in the 200–600 m/z range as well as the protonated molecule, MH^+, and the sodium adduct, MNa^+.

In dynamic RF trapping experiments, spectra were acquired at different time points as the RF field began to increase following the first shut-off. In general, when the laser was fired at increasing RF amplitudes, ions greater than 300 m/z significantly decreased in intensity and were not detected at RF amplitudes greater than ~50% of the set amplitude. The opposite trend was observed for the signal intensities correlating to the F and Y immonium ions. When the laser fired above ~50% of the set amplitude, the low molecular ion signal intensity increased significantly, and the mass

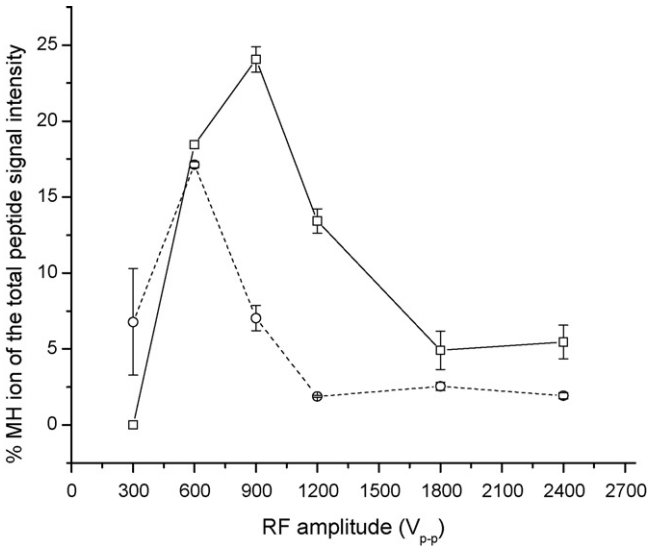

Fig. 7. Percentage of the leucine enkephalin molecular ion to the total peptide signal intensity vs. RF amplitude ($V_{p\text{-}p}$). Circles indicate a constant flow of helium at ~1 mTorr, and squares indicate pulsed gas introduction during the cooling step.

spectra were very similar to those obtained with continuous RF trapping.

The effect of the RF amplitude on the peptide molecular ion signal was also studied. The laser was fired at the same time point (when RF was 0 $V_{p\text{-}p}$) for various RF amplitudes. Fig. 7 shows the percentage of the leucine enkephalin molecular ion at 556 m/z in relation to the total peptide signal. The largest percentage was found at 600 $V_{p\text{-}p}$ with a constant helium buffer gas flow (dashed line). Less fragmentation at 600 $V_{p\text{-}p}$ compared to 2400 $V_{p\text{-}p}$ is related to the ion kinetic energy imparted by the RF field. While a larger well depth is advantageous to trap molecular ions, the higher RF amplitude also imparts a greater kinetic energy which decreases the signal through collision-induced dissociation. The solid line in Fig. 7 shows similar data from a pulsed buffer gas experiment where helium entered the trap only during the cooling step and the flow was turned off during ion extraction. The molecular ion signal intensity was found to be significantly higher with the pulsed gas setup, presumably because the pressure was higher while the flow was on and collisional cooling was more extensive. Taken together, these results show that ion fragmentation in an IT-TOF is highly sensitive to trapping and extraction conditions.

4. Conclusions

The IT-TOF configuration significantly expands the ionization modes that can be used to characterize organic aerosol. In this work, applications to LDI, LD–EI and MALDI were investigated. Some future possibilities include laser desorption–chemical ionization (LD–CI), laser desorption–electron attachment (LD–EA) and the use of MS^n techniques. Field measurements are also feasible as addition of an IT does not significantly increase the footprint of the instrument.

Acknowledgements

The authors thank Katherine Heaton for her help with the α-pinene ozonolysis in the flow tube reactor. This work was supported by the National Science Foundation grant numbers CHE0517972 and CHE0808972.

References

[1] D.M. Murphy, Mass Spectrom. Rev. 26 (2007) 150.
[2] D.G. Nash, T. Baer, M.V. Johnston, Int. J. Mass Spectrom. 258 (2006) 2.
[3] R.C. Sullivan, K.A. Prather, Anal. Chem. 77 (2005) 3861.
[4] S.F. Maria, L.M. Russell, M.K. Gilles, S.C.B. Myneni, Science 306 (2004) 1921.
[5] W.-T. Chen, H. Liao, J.H. Seinfeld, J. Geophys. Res. 112 (2007) D14209.
[6] J. Kaiser, Science 307 (2005) 1858.
[7] B. Oktem, M.P. Tolocka, M.V. Johnston, Anal. Chem. 76 (2004) 253.
[8] M.A. Dreyfus, M.V. Johnston, Aerosol Sci. Technol. 42 (2008) 18.
[9] K.J. Heaton, M.A. Dreyfus, S. Wang, M.V. Johnston, Environ. Sci. Technol. 41 (2007) 6129.
[10] R.E. March, J.F.J. Todd (Eds.), Practical Aspects of Ion Trap Mass Spectrometry, CRC Press, New York, 1995.
[11] A.L. van Wuijckhuijse, M.A. Stowers, W.A. Kleefsman, B.L.M. van Baar, C.E. Kientz, J.C.M. Marijnissen, J. Aerosol Sci. 36 (2005) 677.
[12] W.A. Harris, P.T.A. Reilly, W.B. Whitten, Int. J. Mass Spectrom. 258 (2006) 113.
[13] E.L. McJimpsey, W.M. Jackson, C.B. Lebrilla, H.J. Tobias, M.J. Bogan, E.E. Gard, M. Frank, P.T. Steele, J. Am. Soc. Mass Spectrom. 19 (2008) 315.
[14] Q. Zhang, M.R. Alfarra, D.R. Worsnop, J.D. Allan, H. Coe, M.R. Canagarantna, J.L. Jimenez, Environ. Sci. Technol. 39 (2005) 4938.
[15] S.M. Michael, M. Chien, D.M. Lubman, Rev. Sci. Instrum. 63 (1992) 4277.
[16] D.M. Chambers, L.I. Grace, B.D. Andresen, Anal. Chem. 69 (1997) 3780.
[17] G.L. Klunder, P.M. Grant, B.D. Andresen, R.E. Russo, Anal. Chem. 76 (2004) 1249.
[18] B.M. Chien, S.M. Michael, D.M. Lubman, Rapid Commun. Mass Spectrom. 7 (1993) 837.
[19] D.N. Heller, I. Lys, R.J. Cotter, Anal. Chem. 61 (1989) 1083.
[20] G.L. Glish, D.E. Goeringer, K.G. Asano, S.A. McLuckey, Int. J. Mass Spectrom. Ion Process. 94 (1989) 15.
[21] V. Doroshenko, T.J. Cornish, R.J. Cotter, Rapid Commun. Mass Spectrom. 6 (1992) 753.
[22] G.C. Eiden, M.E. Cisper, M.L. Alexander, P.H. Hemberger, N.S. Nogar, J. Am. Soc. Mass Spectrom. 4 (1993) 706.
[23] G.C. Eiden, A.W. Garrett, M.E. Cisper, N.S. Nogar, P.H. Hemberger, Int. J. Mass Spectrom. Ion Process. 136 (1994) 119.
[24] D.B. Robb, M.W. Blades, Rapid Commun. Mass Spectrom. 13 (1999) 1079.
[25] D.M. Chambers, D.E. Goeringer, S.A. McLuckey, G.L. Glish, Anal. Chem. 65 (1993) 14.
[26] R.R. Vargas, R.A. Yost, in: R.E. March, J.F.J. Todd (Eds.), Practical Aspects of Ion Trap Mass Spectrometry, CRC Press, New York, 1995, p. 217.
[27] M.P. Tolocka, K.J. Heaton, M.A. Dreyfus, S. Wang, C.A. Zordan, T.D. Saul, M.V. Johnston, Environ. Sci. Technol. 40 (2006) 1843.
[28] M.R. Alfarra, D. Paulsen, M. Gysel, A.A. Garforth, J. Dommen, A.S.H. Prevot, D.R. Worsnop, U. Baltensperger, H. Coe, Atmos. Chem. Phys. 6 (2006) 5279.
[29] M.R. Canagaratna, J.T. Jayne, J.L. Jimenez, J.D. Allan, M.R. Alfarra, Q. Zhang, T.B. Onasch, R. Drewnick, H. Coe, A. Middlebrook, A. Delia, L.R. Willams, A.M. Trimborn, M.J. Northway, P.F. DeCarlo, C.E. Kolb, P. Davidovits, D.R. Worsnop, Mass Spectrom. Rev. 26 (2007) 185.
[30] A. McIntosh, T. Donovan, J. Brodbelt, Anal. Chem. 64 (1992) 2079.
[31] V. Doroshenko, R.J. Cotter, J. Mass Spectrom. 31 (1997) 602.
[32] R.J. Cotter, V. Doroshenko, Rapid Commun. Mass Spectrom. 7 (1993) 822.